Peer-reviewed version available at Photonics 2018, 5, 22; doi:10.3390/photonics5030022

Article

Two Types of Localized States in a Photonic Crystal Bounded by an Epsilon Near Zero Nanocomposite

Rashid G. Bikbaev [1,2]*, Stepan Ya. Vetrov [3,4] and Ivan V. Timofeev [4,1]

1 Institute of Nanotechnology, Spectroscopy and Quantum Chemistry, Siberian Federal University, Krasnoyarsk 660041, Russia
2 Polytechnic Institute, Siberian Federal University, Krasnoyarsk 660041, Russia
3 Institute of Engineering Physics and Radio Electronics, Siberian Federal University, Krasnoyarsk 660041, Russia
4 Kirensky Institute of Physics, Federal Research Center KSC SB RAS, Krasnoyarsk 660036, Russia
* Correspondence: Rashid-G-Bikbaev@ya.ru

Version July 6, 2018 submitted to Preprints

Abstract: The spectral properties of a one-dimensional photonic crystal bounded by a resonant absorbing nanocomposite layer with the near-zero permittivity have been studied. The problem of calculating the transmittance, reflectance, and absorptance spectra of such structures at the normal and oblique incidence of light has been solved. It is shown that, depending on the permittivity sign near zero, the nanocomposite is characterized by either metallic or dielectric properties. For the first time, the possibility of simultaneous formation of the Tamm plasmon polariton at the photonic crystal/metallic nanocomposite interface and the localized state similar to the defect mode with the field intensity maximum inside the dielectric nanocomposite layer is demonstrated. Specific features of field localization at the Tamm plasmon polariton and defect mode frequencies are analyzed.

Keywords: photonic crystal, nanocomposite, epsilon near zero material, Tamm plasmon polariton

1. Introduction

A special type of surface electromagnetic states in the form of a standing surface wave with the zero wavenumber along the interface between media, which does not transfer energy, have recently been in focus of researchers. In this case, the wave equation following from the Maxwell equations for an electric field is the exact analog of the one-electron Schrödinger equation for a semi-infinite crystal, the solution of which is the electronic Tamm state [1]. Therefore, the electromagnetic analog of the electronic Tamm state at the normal incidence of light onto a sample is called the optical Tamm state (OTS). If such a state exists at the interface between a photonic crystal (PhC) and a conducting medium with the effective permittivity $\Re\varepsilon_{eff}(\omega) < 0$, the light wave interacts with a surface plasmon, i.e., the collective oscillation of the free electron gas at the conductor surface. The result of interaction between the radiation field and surface plasmon excitation is a Tamm plasmon polariton (TPP) [2], which is observed in experiments as a narrow peak in the energy spectra of a sample [3–5]. As was shown in [6–10], the materials with the negative permittivity ($\Re\varepsilon_{eff}(\omega) < 0$) adjacent to a PhC can be both metallic films and nanocomposites with the resonant frequency dispersion.

Theoretical and experimental investigations of the properties of TPPs allowed them to be used as a basis of the fundamentally new class of devices, including absorbers [11–14], switchers [15], organic solar cells [16], thermal emitters [17,18], sensors [19–21], and spontaneous radiation amplifiers [22]. The high degree of field localization at the TPP frequency makes it possible to reduce the threshold of generation of nonlinear effects [23–25] and implement the extremely high light transmission through a nanohole [26]. The interaction of the TPPs with other types of localized modes allows lasers [27,28], single-photon sources [29], and electro-optically tunable Tamm plasmon-polariton-excitons [30] to be obtained. In [31,32], we found the localized state in the structure containing a cholesteric liquid crystal. Later on, a chiral analog of the TPP in a cholesteric liquid crystal was established [33]. In this case, the

polarization-preserving anisotropic mirror made of a metal-dielectric nanocomposite was used as a metallic layer [34].

Of great interest are materials with the near-zero permittivity. Such structures are used to control the wave front shape [35], enhance the transmission of light through a subwavelength aperture [36] and nonlinear effects [37,38], develop absorbers [39], photonic wires [40], and insulators [41], and perform the third-harmonic generation [42]. The materials with the near-zero permittivity involve layered plasmon structures, indium tin oxide (ITO), metal-dielectric, and polymer nanocomposites, and composites with core-shell nanoparticles. In this work, we demonstrate the possibility of simultaneous implementation of the TPP and defect mode localized at the interface between a PhC and a nanocomposite with the near-zero effective permittivity [43]. The nanocomposite consists of metallic nanoparticles dispersed in a transparent matrix and has the resonant effective permittivity. The optical characteristics of initial materials have no resonant features [44–46]. The position of a frequency band corresponding to the near-zero effective permittivity is determined by the permittivities of initial materials and volume concentration of nanoparticles. This opens wide opportunities for guiding the optical properties of localized state.

2. Model Description and Determining the Transmittance

We consider a PhC structure in the form of a layered medium bounded by a nanocomposite layer with finite thickness (Fig. 1). The PhC unit cell is formed of materials a and b with respective layer thicknesses d_a and d_b and permittivities ε_a and ε_b.

The nanocomposite layer with thickness d_{eff} consists of spherical metallic nanoparticles uniformly distributed in a dielectric matrix.

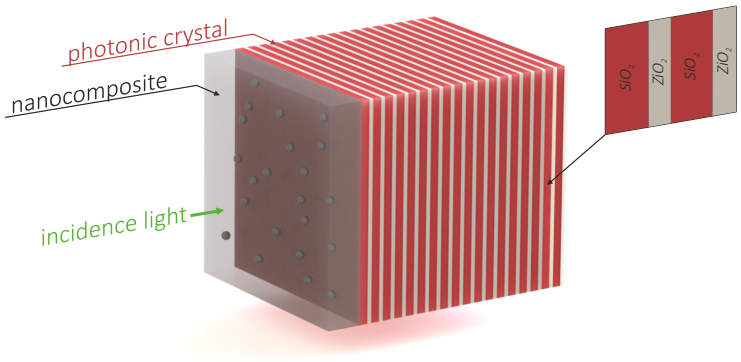

Figure 1. Schematic of a one-dimensional PhC bounded by a nanocomposite layer.

Hereinafter, we assume the PhC structure to be placed in vacuum.

The effective permittivity of the nanocomposite is determined using the Maxwell Garnett formula [47,48] widely used in studying matrix media, in which isolated metallic inclusions with a small volume fraction are dispersed in the matrix material

$$\varepsilon_{eff} = \varepsilon_d \left[1 + \frac{f\left(\varepsilon_m(\omega) - \varepsilon_d\right)}{\varepsilon_d + (1-f)\left(\varepsilon_m(\omega) - \varepsilon_d\right)1/3} \right] \tag{1}$$

where f is the filling factor, i.e., the fraction of nanoparticles in the matrix; ε_d and $\varepsilon_m(\omega)$ are the permittivities of the matrix glass and nanoparticle metal, respectively; and ω is the radiation frequency.

The Maxwell Garnett model suggests the quasi-steady-state approximation. The model has the following specific features: the nanocomposite layer is electrodynamically isotropic and the size of inclusions and distance between them are much smaller than the optical wavelength in the

investigated effective medium. We determine the permittivity of a nanoparticle metal using the Drude approximation

$$\varepsilon_m(\omega) = \varepsilon_0 - \frac{\omega_p^2}{\omega(\omega + i\gamma)}, \tag{2}$$

where ε_0 is the constant taking into account the contributions of interband transitions of bound electrons; ω_p is the plasma frequency; γ is the reciprocal electron relaxation time.

The change in the light field upon its passing through each structural layer is determined by the transfer matrix metod [49].

3. Results and Discussion

We investigate the localized states formed at the PhC/nanocomposite interface. The nanocomposite consists of metallic nanospheres dispersed in a dielectric matrix and is characterized by the resonant effective permittivity

$$\varepsilon_{eff}(\omega) = \Re\varepsilon_{eff}(\omega) + i\Im\varepsilon_{eff}(\omega). \tag{3}$$

In approximation $\gamma \ll \omega$ it follows from Eq. (1) that the real part of the effective permittivity at nonzero f takes the zero value at two points with the frequencies

$$\omega_0 = \omega_p\sqrt{\frac{1-f}{3\varepsilon_d + (1-f)(\varepsilon_0 - \varepsilon_d)}}, \quad \omega_1 = \omega_p\sqrt{\frac{1+2f}{(\varepsilon_0 + 2\varepsilon_d + 2f(\varepsilon_0 - \varepsilon_d))}}. \tag{4}$$

In the range of $[\omega_0, \omega_1]$, the nanocomposite is similar to the metal. It means that, in this frequency range, the TPP can exist at the PhC/nanocomposite interface. At $\omega > \omega_1$, the nanocomposite plays the role of a dielectric layer with $\Re\varepsilon_{eff}(\omega) > 0$ and $\Im\varepsilon_{eff}(\omega) \ll 1$ and, as we show below, the localized (defect) mode with the electric field intensity maximum inside the layer can exist along with the TPP.

In our structure, the materials of alternating PhC layers are silicon dioxide (SiO_2) with a permittivity of $\varepsilon_a = 2.10$ and zirconium dioxide (ZrO_2) with a permittivity of $\varepsilon_b = 4.16$. The respective layer thicknesses are $d_a = 74$ nm and $d_b = 50$ nm and the number of layers is $N = 21$.

The epsilon near zero nanocomposite layer with a thickness of $d_{eff} = 300$ nm consists of silver nanospheres dispersed in the transparent optical glass. The parameters of silver are $\varepsilon_0 = 5$, $\omega_p = 9$ eV, and $\gamma = 0.02$ eV and the permittivity of glass is $\varepsilon_d = 2.56$. The frequency dependences of the real and imaginary parts of permittivity calculated using formula (1) show that, as the volume concentration of the nanospheres in the nanocomposite film increases, the frequency ω corresponding to the collective plasmon resonance shifts to the low-frequency region. In this case, the half-width of the $\Im\varepsilon_{eff}(\omega)$ resonance curve changes insignificantly, the $\Re\varepsilon_{eff}(\omega)$ curve is noticeably modified, and the frequency range corresponding to $\Re\varepsilon_{eff}(\omega) < 0$ broadens out. As an example, Fig. 2 shows the $\Im\varepsilon_{eff}(\omega)$ and $\Re\varepsilon_{eff}(\omega)$ curves at $f = 0.11$, together with the transmittance, reflectance, and absorbance spectra of a PhC conjugated with a nanocomposite film. The PhC band gap is limited by a frequency range of $0.26\,\omega/\omega_p < \omega < 0.39\,\omega/\omega_p$.

It can be seen in Fig. 2 that near the high-frequency boundary of the PhC band gap, the absorption bands arise, which correspond to the localized states formed at the PhC/nanocomposite interface. The low-frequency state ($\lambda = 406.5$ nm) exists in the range with $\Re\varepsilon_{eff}(\omega) < 0$ (TPP) and the high-frequency state ($\lambda = 395.6$ nm), in the range with $\Re\varepsilon_{eff}(\omega) > 0$ (defect mode). At the TPP frequency, the effective permittivity takes the values of $\varepsilon_{eff}(\omega) = -0.0485 + 0.0892i$ and, at the defect mode frequency, $\varepsilon_{eff}(\omega) = 0.5474 + 0.0570i$.

The electric field intensity distribution at the corresponding frequencies of the localized states at the contact between the PhC and nanocomposite film is illustrated in Fig. 3.

Preprints (www.preprints.org) | NOT PEER-REVIEWED | Posted: 6 July 2018 doi:10.20944/preprints201807.0109.v1

Peer-reviewed version available at Photonics 2018, 5, 22; doi:10.3390/photonics5030022

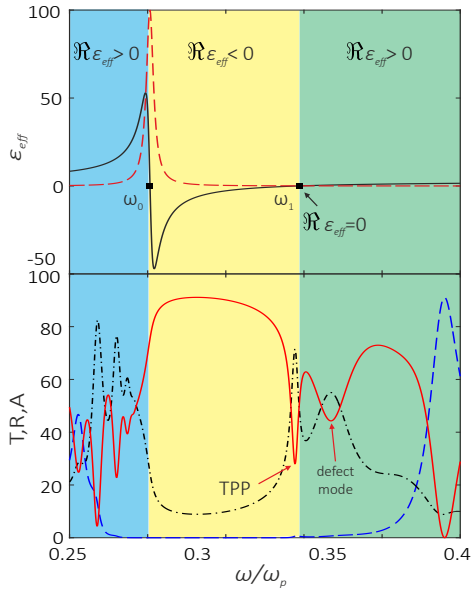

Figure 2. Dependences of the imaginary $\Im\varepsilon_{eff}(\omega)$ (dashed line) and real $\Re\varepsilon_{eff}(\omega)$ (solid line) parts of the effective permittivity $\varepsilon_{eff}(\omega)$ on normalized frequency ω/ω_p (on the top) and transmittance (dashed line), reflectance (solid line) and absorbance (dash-and-dot line) spectra of the PhC/nanocomposite structure at the normal incidence of light onto it (Fig. 1). The nanocomposite layer thickness is $d_{eff} = 300$ nm and $f = 0.11$.

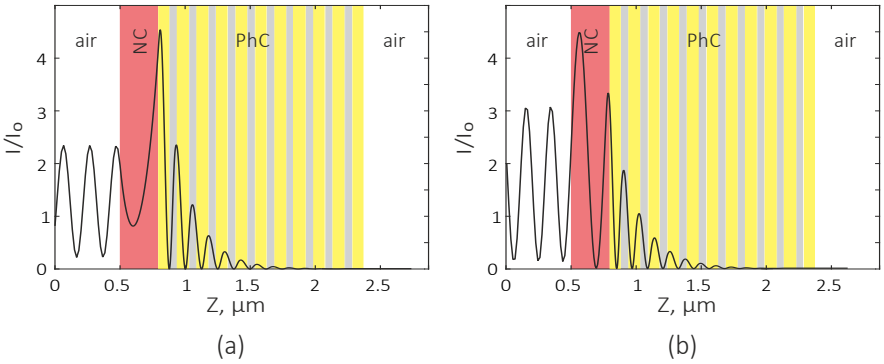

Figure 3. Schematic of a one-dimensional PhC conjugated with the nanocomposite layer and field intensity distribution at the frequencies of (a) TPP and (b) defect mode normalized to the input intensity. The nanocomposite layer thickness is $d_{eff} = 300$ nm and $f = 0.11$.

It can be seen in Fig. 3 that for the TPP the field is localized at the PhC/nanocomposite interface and for the defect mode, in the bulk of the nanocomposite layer.

The localization values are almost the same. In both cases, the light field in the states is localized in the region comparable with the wavelength.

The change in the nanocomposite filling factor is a powerful tool for frequency tuning. The reflectance spectra of the investigated structure calculated at different nanocomposite filling factors are shown in Fig. 4.

It can be seen in Fig. 4 that the increase in the volume concentration of metallic inclusions in the bulk of nanocomposite leads to the shift of localized states to the high-frequency region. In this case, the frequency range between the TPP and defect mode reflection minima also increases. Note that with an increase in the filing factor, the reflectance at the TPP frequency increases. According to the

Preprints (www.preprints.org) | NOT PEER-REVIEWED | Posted: 6 July 2018 doi:10.20944/preprints201807.0109.v1

Peer-reviewed version available at Photonics 2018, 5, 22; doi:10.3390/photonics5030022

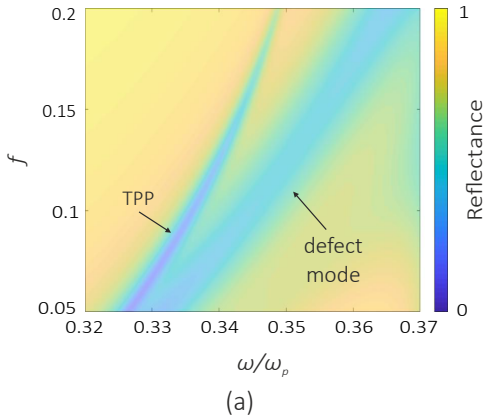

Figure 4. Reflectance spectra of the PhC/nanocomposite structure at the normal incidence of light onto the sample at different nanocomposite filling factors. The nanocomposite layer thickness is $d_{eff} = 300$ nm.

energy conservation law, the absorption in the nanocomposite layer decreases and can be controlled by changing the layer thickness.

Reflectance spectra of the PhC/nanocomposite structure with different nanocomposite film thicknesses are presented in Fig. 5.

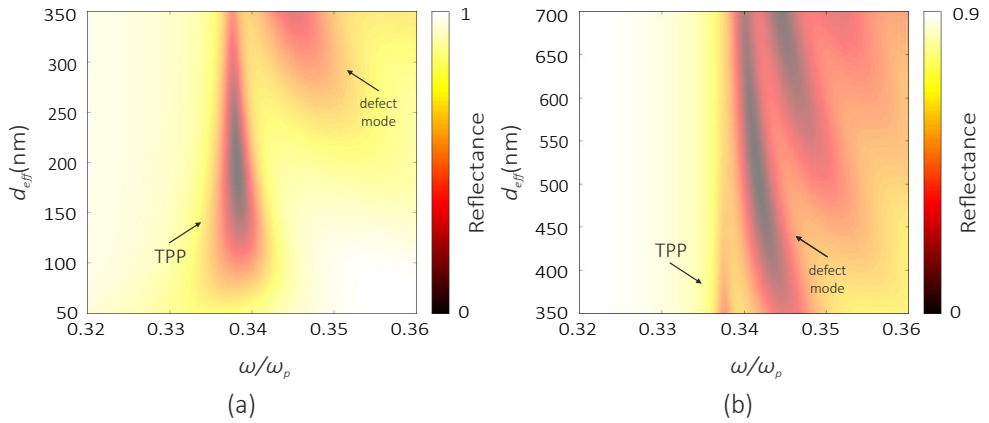

Figure 5. Reflectance spectra of the PhC/nanocomposite structure at the normal incidence of light onto the sample with nanocomposite film thicknesses in the ranges of (a) 50 nm $< d_{eff} <$ 350 nm and (b) 350 nm $< d_{eff} <$ 700 nm. The filling factor is $f = 0.11$.

The change in the nanocomposite layer thickness leads to the significant variation in the reflectance spectrum in the frequency range near $\varepsilon = 0$. In particular, in the nanocomposite film with a thickness of up to 250 nm, only the TPP exists. The reflectance minimum is observed at a thickness of $d_{eff} = 200$ nm (Fig. 5a). The use of nanocomposite films thicker than 250 nm leads to the formation of a defect mode and corresponding second reflectance gap. The second reflectance minimum corresponds to a thickness of $d_{eff} = 520$ nm. It should be noted that at $d_{eff} > 400$ nm, the TPP does not exist (Fig. 5b).

The calculations show that the defect mode is an eigenmode of the Fabry-Pérot dielectric resonator, which is represented by a nanocomposite enclosed between the PhC and the vacuum half-space. For such a resonator, we can write

$$n_{eff} d_{eff} = N\lambda/2, \tag{5}$$

where N is the mode number.

Preprints (www.preprints.org) | NOT PEER-REVIEWED | Posted: 6 July 2018 doi:10.20944/preprints201807.0109.v1

Peer-reviewed version available at Photonics 2018, 5, 22; doi:10.3390/photonics5030022

At a frequency of $\omega = 0.3472\omega_p$ and a permittivity of $\varepsilon_{eff}(\omega) = 0.5474 + 0.0570i$, the wavelength is $\lambda = 444.5$ nm in vacuum and, according to Eq. (5), $\lambda_{eff} = \lambda / n_{eff} = 600$ nm in the nanocomposite layer; therefore, the thickness $d_{eff} = 300$ nm corresponds to half-wavelength condition Eq. (5).

Figure 6 shows reflectance spectra of the structure in dependence of PhC first-layer thickness d_{first}. The thickness variation can be ensured by forming a sharp-wedge-shaped layer [50]. In this case, an insignificant destruction of plane-parallelism of the layers can be compensated by a correct choice of the optical beam width.

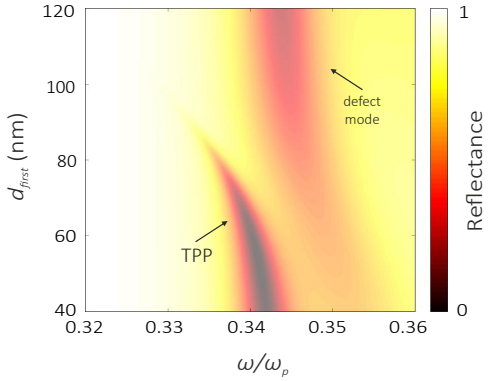

Figure 6. Reflectance spectra of the PhC/nanocomposite structure at the normal incidence of light onto the sample at different PhC first-layer thicknesses. The filling factor is $f = 0.11$ and $d_{eff} = 300$ nm.

It can be seen in Fig. 6 that the frequency positions of the localized states and distance between them significantly change upon variation in the first-layer thickness d_{first}. The increase in d_{first} leads to the shift of the TPP and defect mode frequencies toward longer wavelengths. In this case, a sort of switching between the TPP and defect mode is implemented. It can be seen that the defect mode exists when the first-layer thickness is larger than 85 nm; in this case, the TPP does not exist.

Such a switching from the TPP to defect mode upon variation in the PhC first-layer thickness makes these structures promising for application in tunable filters and sensors.

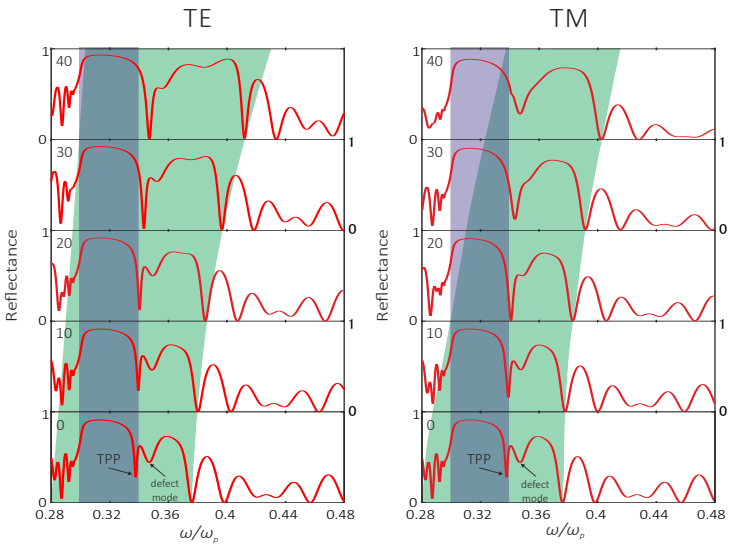

Figure 7. Angular and frequency dependences of the reflectance spectra of the PhC/nanocomposite structure for the TE and TM modes. The filling factor is $f = 0.11$ and $d_{eff} = 300$ nm. Purple and green fillings denote the $\Re\varepsilon_{eff} < 0$ and photonic band gap respectively.

Preprints (www.preprints.org) | NOT PEER-REVIEWED | Posted: 6 July 2018 doi:10.20944/preprints201807.0109.v1

Peer-reviewed version available at Photonics 2018, 5, 22; doi:10.3390/photonics5030022

Along with the aforesaid, one of the effective ways of controlling the energy spectra is changing the angle of incidence of light onto a sample. Study of the reflectance spectra showed that for the TE modes the increase in the angle of incidence leads to the broadening of the initial PhC band gap and its shift to the high-frequency range (Fig. 7).

It is noteworthy that the overlap of the region with $\Re\varepsilon_{eff}(\omega) < 0$ and the band gap is observed over the entire range of investigated angles. However, the TPP does not exist at angles over 30 degrees. This is due to the fact that the increase in the angle of incidence leads to the TPP shift to the high-frequency region, crossing the point $\omega = \omega_1$, and TPP transformation to the defect mode.

The different picture is observed for the TM waves. The increase in the angle of incidence leads to the stronger shift of the PhC band gap to the high-frequency region than in the case of TE modes. At angles more than 40 degrees, the region with $\Re\varepsilon_{eff}(\omega) < 0$ and PhC band gap stop overlapping. In this case, the TPP does not exist, as for the TE modes, at angles over 30 degrees.

3.1. Fresnel reflection from a nanocomposite film

Let us clarify the nature of formation of the localized states at the small negative and positive nanocomposite permittivities. We calculate the Fresnel reflectance from the nanocomposite film with finite thickness [51].

The reflectances at the first and second film boundaries are

$$r_{12} = \frac{n_1 - n_2}{n_1 + n_2}, \quad r_{23} = \frac{n_2 - n_3}{n_2 + n_3}, \tag{6}$$

where n_1 and n_3 are the refractive indices of the media surrounding the nanocomposite film, $n_2 = \sqrt{\varepsilon_{eff}}$.

The total reflectance is determined as:

$$R = \left| \frac{r_{12} + r_{23}e^{2i\beta}}{1 + r_{12}r_{23}e^{2i\beta}} \right|^2 = \frac{r_{12}^2 + r_{23}^2 + 2r_{12}r_{23}\cos(2\beta)}{1 + r_{12}^2 r_{23}^2 + 2r_{12}r_{23}\cos(2\beta)}, \tag{7}$$

where $\beta = \frac{2\pi}{\lambda_0} n_2 d_{eff}$, and d_{eff} is the nanocomposite film thickness.

Figure 8 shows the calculated dependence of the Fresnel reflectance on the nanocomposite layer thickness d_{eff} at the normal incidence of light onto the nanocomposite.

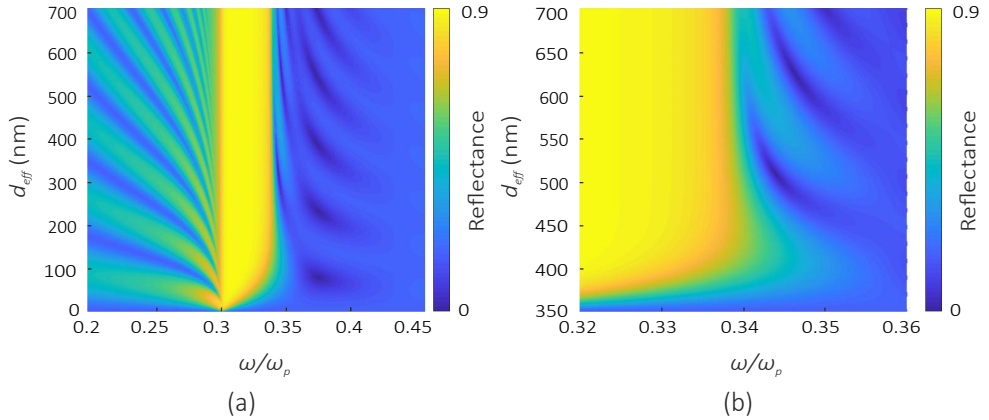

Figure 8. Fresnel reflectance at the nanocomposite/silicon dioxide interface. The nanocomposite filling factor is $f = 0.11$.

It can be seen in Fig. 8a that at a nanocomposite film thickness of 300 nm at the TPP frequency ($\omega = 0.3378\omega_p$), the Fresnel reflectance from the nanocomposite attains 58%, which facilitates the localized state formation at the PhC/nanocomposite interface. At the same nanocomposite film thickness at a defect mode frequency $\omega = 0.3472\omega_p$, the reflectance is about 5%.

Preprints (www.preprints.org) | NOT PEER-REVIEWED | Posted: 6 July 2018 doi:10.20944/preprints201807.0109.v1

Peer-reviewed version available at Photonics 2018, 5, 22; doi:10.3390/photonics5030022

At $R \to 0$ the local intensity of the field at the TPP frequency decreases. And contrariwise at the defect mode frequency it grows up. The reflection zero condition $R = 0$ can be written in account of Eq. (7):

$$r_{12}^2 + r_{23}^2 + 2r_{12}r_{23}\cos(2\beta) = 0 \Rightarrow \cos(2\beta) = -\frac{r_{12}^2 + r_{23}^2}{2r_{12}r_{23}} \Rightarrow \cos\left(\frac{3\pi}{\lambda_0} n_2 d_{eff}\right) = -\frac{r_{12}^2 + r_{23}^2}{2r_{12}r_{23}}.$$

Using this equations, we can express $d_{eff}(\omega, n_{1,3}, n_2(\omega))$; this is a complex quantity, which will have the form

$$d_{eff}(\omega, n_{1,3}, n_2(\omega)) = \arccos\left(-\frac{r_{12}^2 + r_{23}^2}{2r_{12}r_{23}}\right)\frac{\lambda_0}{3\pi n_2}. \quad (8)$$

Equation (8) can be built numerically or graphically; then, the number of varied parameters will increase to 3, since, along with the variation in the incident radiation frequency and nanocomposite layer thickness, we can change the nanocomposite filling factor. This allows us to solve Eq. (8) at zero reflectance (7) at the frequencies corresponding to the near-zero effective permittivity of the nanocomposite. It was established that this condition is satisfied at $f = 0.25\%$ (Fig. 9).

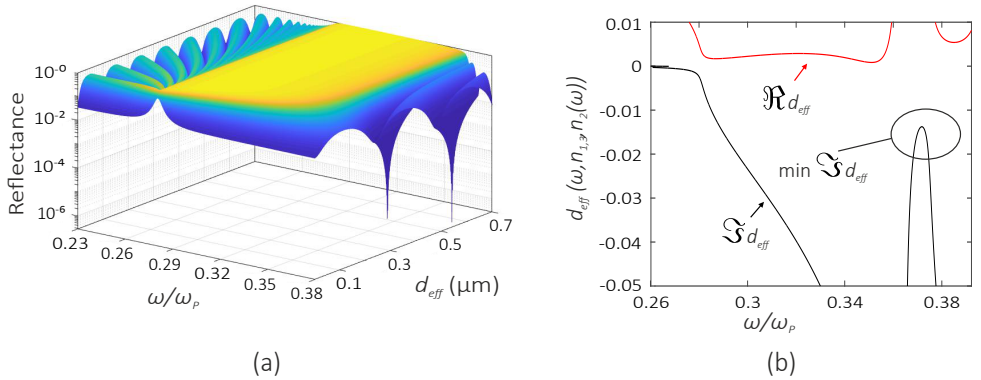

Figure 9. Graphic solution of Eq. (7) (a) and Eq. (8) (b) at a nanocomposite filling factor of $f = 0.25$.

It can be seen in Fig. 9a that in the investigated nanocomposite layer thickness range, there are two solutions at frequencies of $\omega_1 = 0.3713\omega_p$ and $\omega_2 = 0.3747\omega_p$. In this case, $d_{eff} = 341$ and 576 nm, respectively.

It should be noted that, in this case, condition (5) is also met, since at a frequency of $\omega_1 = 0.3713\omega_p$ and $\varepsilon_{eff}(\omega_1) = 0.2897 + 0.03867i$ the wavelength is $\lambda = 369$ nm in vacuum and $\lambda_{eff} = 685$ nm in the nanocomposite layer; therefore, the thickness $d_{eff} = 341$ nm is almost consistent with the half-wavelength condition ($N = 1$ in Eq. (5)). At a frequency of $\omega_2 = 0.3747\omega_p$ and $\varepsilon_{eff}(\omega_2) = 0.4024 + 0.03582i$, the wavelength is $\lambda = 366$ nm in vacuum and $\lambda_{eff} = 577$ nm in the nanocomposite layer. Thus, the thickness $d_{eff} = 576$ nm is almost consistent with the wavelength in the medium ($N = 2$ in Eq. (5)).

The graphic analysis of Eq. (8) showed that in the frequency range of the near-zero permittivity, there is no exact solution. However, in this range, the imaginary part of d_{eff} takes the minimum values (Fig. 9b). Thus, Eqs. (7) and (8) have the analogous solutions.

3.2. Coupled mode theory

The principle of defect mode formation can be explained using the coupled mode theory. According to this theory, the defect mode formation involves the contributions of three energy channels, each characterized by relaxation rate γ. The relaxation rate is equal to the ratio between the total power of energy relaxation and the energy accumulated in the defect mode. We denote the rates of energy relaxation to the transmission and absorption channels of the nanocomposite film and the transmission channel of the PhC by $\gamma_{Fresnel}$, γ_A, and γ_{PhC}, respectively. The energy accumulated in the defect layer is

Peer-reviewed version available at Photonics 2018, 5, 22; doi:10.3390/photonics5030022

the same for determining the rate of relaxation to each channel. Therefore, the ratio between relaxation rates is determined by the ratio between powers of leakage to the channels and can be related to the energy coefficients of the structure as [18]:

$$\gamma_{Fresnel} : \gamma_A : \gamma_{PhC} \Leftrightarrow \left(1 - r_{12}^2\right) : A : T_{\mathrm{PhC}} \tag{9}$$

In this case, the energy accumulated in the defect mode will be maximal under the critical coupling condition

$$\gamma_{Fresnel} = \gamma_A + \gamma_{PhC} \Leftrightarrow \left(1 - r_{12}^2\right) = A + T_{PhC}. \tag{10}$$

The graphic verification of the validity of critical coupling conditions (10) at nanocomposite layer thicknesses of $d_{eff} = 341$ and 576 nm is illustrated in Fig. (10).

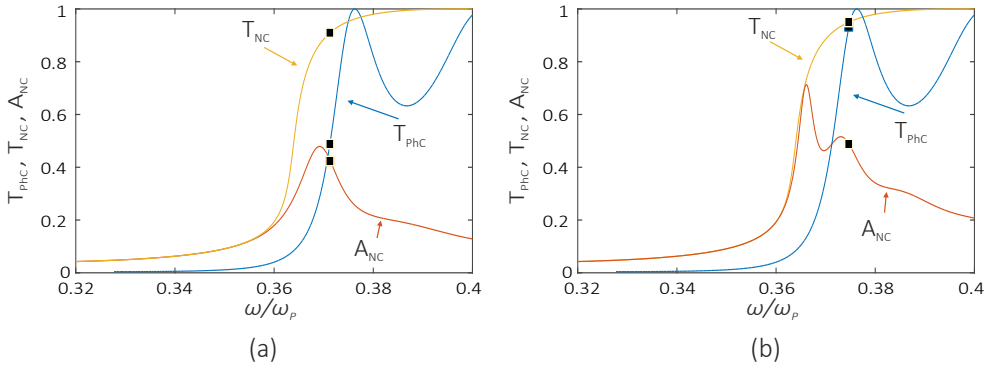

Figure 10. Graphic solution of critical coupling condition (10) at a nanocomposite layer thickness of 341 nm (on the top) and 576 nm (in the bottom). The nanocomposite filling factor is $f = 0.25$.

Note that at a wavelength of $d_{eff} = 341$ nm, condition (10) is valid, while at $d_{eff} = 576$ nm, it is invalid. This can be explained by the low Q factor of the resonator mode at $d_{eff} = 576$ nm. In this case, the coupled mode theory allows the process to be only qualitatively, yet not quantitatively, described [52].

To check the validity of the critical coupling conditions for the TPP in the case of a PhC conjugated with the 341-nm thick nanocomposite, we write the expression analogous to (10):

$$\gamma_{NC} = \gamma_A; \gamma_{PhC} = 0 \Leftrightarrow T_{NC} = A_{NC}; T_{PhC} = 0. \tag{11}$$

Analysis of the energy spectra of the structure showed that at the TPP from the nanocomposite film side, condition (11) is not met because of the weak coupling of the incident radiation with the TPP (Fig. 11).

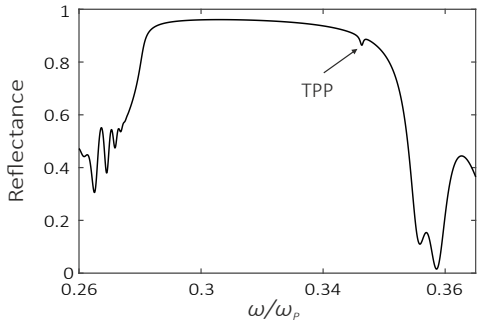

Figure 11. Reflectance spectra of the structure for the radiation incident from the nanocomposite layer side. $d_{eff} = 341$ nm and $f = 0.25$.

However, the coupled mode theory makes it possible to estimate the reflectance value relative to the background radiation at the frequency of the TPP excited from the nanocomposite side:

$$r_{(NC-PhC)} = \rho^2_{(NC-PhC)} = \left(-1 + \frac{2\gamma_{NC}}{\sum\limits_i \gamma_i} \right)^2 . \quad (12)$$

The transfer-matrix results and coupled mode theory data are given in Table 1.

Table 1. Coefficients of reflection at the frequency of the TPP

Method	Reflectance
Transfer martix	0.9694
CMT	0.9693

Thus, the coupled mode theory gives a good agreement with the transfer matrix method.

4. Conclusions

We examined the spectral properties of a one-dimensional photonic crystal conjugated with the resonant absorbing nanocomposite layer consisting of spherical silver nanoparticles dispersed in transparent optical glass. We showed first that in the frequency band where the effective permittivity takes near-zero values, the nanocomposite exhibits the properties of both a metal and a dissipative dielectric. As a result, both the Tamm plasmon polariton and defect mode exist at the photonic crystal/nanocomposite interface. We demonstrated that the field localization at the Tamm plasmon polariton and defect mode frequencies can be the same. We established the nanocomposite film thicknesses at which both modes can simultaneously exist in the structure. We showed that the frequency positions of the modes can be effectively controlled by varying the thickness of a photonic crystal layer adjacent to the nanocomposite and the nanocomposite filling factor. The obtained results scale up possible implementations of Tamm plasmon polaritons in resonant photonic crystal structures.

5. Acknowledgment

The reported study was funded by RFBR according to the research projects No 18-32-00053 and by Russian Foundation for Basic Research, Government of Krasnoyarsk Territory, Krasnoyarsk Region Science and Technology Support Fund to the research project No 17-42-240464.

1. Tamm, I.E. Tamm_t1_1975ru.pdf. *Phys. Z. Sowjetunion* **1932**, *1*, 733.
2. Kaliteevski, M.A.; Iorsh, I.; Brand, S.; Abram, R.A.; Chamberlain, J.M.; Kavokin, A.V.; Shelykh, I.A. Tamm plasmon-polaritons: Possible electromagnetic states at the interface of a metal and a dielectric Bragg mirror. *Physical Review B* **2007**, *76*, 165415. doi:10.1103/PhysRevB.76.165415.
3. Goto, T.; Dorofeenko, A.V.; Merzlikin, A.M.; Baryshev, A.V.; Vinogradov, A.P.; Inoue, M.; Lisyansky, A.A.; Granovsky, A.B. Optical tamm states in one-dimensional magnetophotonic structures. *Physical Review Letters* **2008**, *101*, 14–16, [0802.3192]. doi:10.1103/PhysRevLett.101.113902.
4. Sasin, M.E.; Seisyan, R.P.; Kaliteevski, M.A.; Brand, S.; Abram, R.A.; Chamberlain, J.M.; Egorov, A.Y.; Vasil'ev, A.P.; Mikhrin, V.S.; Kavokin, A.V. Tamm plasmon polaritons: Slow and spatially compact light. *Applied Physics Letters* **2008**, *92*, 251112. doi:10.1063/1.2952486.
5. Sasin, M.E.; Seisyan, R.P.; Kaliteevski, M.A.; Brand, S.; Abram, R.A.; Chamberlain, J.M.; Iorsh, I.V.; Shelykh, I.A.; Egorov, A.Y.; Vasil'ev, A.P.; Mikhrin, V.S.; Kavokin, A.V. Tamm plasmon-polaritons: First experimental observation. *Superlattices and Microstructures* **2010**, *47*, 44–49. doi:10.1016/j.spmi.2009.09.003.
6. Vetrov, S.Y.; Bikbaev, R.G.; Timofeev, I. Optical Tamm states at the interface between a photonic crystal and a nanocomposite with resonance dispersion. *Journal of Experimental and Theoretical Physics* **2013**, *117*, 988–998. doi:10.1134/S1063776113140185.

7. Vetrov, S.Y.; Bikbaev, R.G.; Timofeev, I. The optical Tamm states at the edges of a photonic crystal bounded by one or two layers of a strongly anisotropic nanocomposite. *Optics Communications* **2017**, *395*, 275–281. doi:10.1016/j.optcom.2016.08.075.
8. Vetrov, S.Y.; Pankin, P.S.; Timofeev, I. The optical Tamm states at the interface between a photonic crystal and a nanocomposite containing core–shell particles. *Journal of Optics* **2016**, *18*, 065106. doi:10.1088/2040-8978/18/6/065106.
9. Bikbaev, R.G.; Vetrov, S.Y.; Timofeev, I. The optical Tamm states at the interface between a photonic crystal and nanoporous silver. *Journal of Optics* **2017**, *19*, 015104. doi:10.1088/2040-8986/19/1/015104.
10. Bikbaev, R.G.; Vetrov, S.Y.; Timofeev, I. Optical Tamm states at the interface between a photonic crystal and a gyroid layer. *Journal of the Optical Society of America B* **2017**, *34*, 2198. doi:10.1364/JOSAB.34.002198.
11. Gong, Y.; Liu, X.; Wang, L.; Lu, H.; Wang, G. Multiple responses of TPP-assisted near-perfect absorption in metal/Fibonacci quasiperiodic photonic crystal. *Optics Express* **2011**, *19*, 9759. doi:10.1364/OE.19.009759.
12. Gong, Y.; Liu, X.; Lu, H.; Wang, L.; Wang, G. Perfect absorber supported by optical Tamm states in plasmonic waveguide. *Optics Express* **2011**, *19*, 18393. doi:10.1364/OE.19.018393.
13. Fang, M.; Shi, F.; Chen, Y. Unidirectional All-Optical Absorption Switch Based on Optical Tamm State in Nonlinear Plasmonic Waveguide. *Plasmonics* **2016**, *11*, 197–203. doi:10.1007/s11468-015-0042-z.
14. Xue, C.H.; Wu, F.; Jiang, H.T.; Li, Y.; Zhang, Y.W.; Chen, H. Wide-angle Spectrally Selective Perfect Absorber by Utilizing Dispersionless Tamm Plasmon Polaritons. *Scientific Reports* **2016**, *6*, 39418. doi:10.1038/srep39418.
15. Zhang, W.; Yu, S. Bistable switching using an optical Tamm cavity with a Kerr medium. *Optics Communications* **2010**, *283*, 2622–2626. doi:10.1016/j.optcom.2010.02.035.
16. Zhang, X.L.; Song, J.F.; Li, X.B.; Feng, J.; Sun, H.B. Optical Tamm states enhanced broad-band absorption of organic solar cells. *Applied Physics Letters* **2012**, *101*, 243901. doi:10.1063/1.4770316.
17. Yang, Z.Y.; Ishii, S.; Yokoyama, T.; Dao, T.D.; Sun, M.G.; Nagao, T.; Chen, K.P. Tamm plasmon selective thermal emitters. *Optics Letters* **2016**, *41*, 4453. doi:10.1364/OL.41.004453.
18. Yang, Z.Y.; Ishii, S.; Yokoyama, T.; Dao, T.D.; Sun, M.G.; Pankin, P.S.; Timofeev, I.; Nagao, T.; Chen, K.P. Narrowband Wavelength Selective Thermal Emitters by Confined Tamm Plasmon Polaritons. *ACS Photonics* **2017**, *4*, 2212–2219. doi:10.1021/acsphotonics.7b00408.
19. Huang, S.G.; Chen, K.P.; Jeng, S.C. Phase sensitive sensor on Tamm plasmon devices. *Optical Materials Express* **2017**, *7*, 1267. doi:10.1364/OME.7.001267.
20. Auguié, B.; Fuertes, M.C.; Angelomé, P.C.; Abdala, N.L.; Soler Illia, G.J.A.A.; Fainstein, A. Tamm Plasmon Resonance in Mesoporous Multilayers: Toward a Sensing Application. *ACS Photonics* **2014**, *1*, 775–780. doi:10.1021/ph5001549.
21. Kumar, S.; Shukla, M.K.; Maji, P.S.; Das, R. Self-referenced refractive index sensing with hybrid-Tamm-plasmon-polariton modes in sub-wavelength analyte layers. *Journal of Physics D: Applied Physics* **2017**, *50*, 375106. doi:10.1088/1361-6463/aa7fd7.
22. Gubaydullin, A.R.; Symonds, C.; Bellessa, J.; Ivanov, K.A.; Kolykhalova, E.D.; Sasin, M.E.; Lemaitre, A.; Senellart, P.; Pozina, G.; Kaliteevski, M.A. Enhancement of spontaneous emission in Tamm plasmon structures. *Scientific Reports* **2017**, *7*, 9014. doi:10.1038/s41598-017-09245-7.
23. Vinogradov, A.P.; Dorofeenko, A.V.; Erokhin, S.G.; Inoue, M.; Lisyansky, A.A.; Merzlikin, A.M.; Granovsky, A.B. Surface state peculiarities in one-dimensional photonic crystal interfaces. *Physical Review B* **2006**, *74*, 045128. doi:10.1103/PhysRevB.74.045128.
24. Xue, C.H.; Jiang, H.T.; Lu, H.; Du, G.Q.; Chen, H. Efficient third-harmonic generation based on Tamm plasmon polaritons. *Optics letters* **2013**, *38*, 959–61. doi:10.1364/OL.38.000959.
25. Afinogenov, B.I.; Bessonov, V.O.; Fedyanin, A.A. Second-harmonic generation enhancement in the presence of Tamm plasmon-polaritons. *Optics Letters* **2014**, *39*, 6895. doi:10.1364/OL.39.006895.
26. Treshin, I.V.; Klimov, V.V.; Melentiev, P.N.; Balykin, V.I. Optical Tamm state and extraordinary light transmission through a nanoaperture. *Physical Review A* **2013**, *88*, 023832, [arXiv:1305.4340v1]. doi:10.1103/PhysRevA.88.023832.
27. Symonds, C.; Lheureux, G.; Hugonin, J.P.; Greffet, J.J.; Laverdant, J.; Brucoli, G.; Lemaitre, A.; Senellart, P.; Bellessa, J. Confined Tamm Plasmon Lasers. *Nano Letters* **2013**, *13*, 3179–3184. doi:10.1021/nl401210b.

28. Symonds, C.; Lemaître, A.; Senellart, P.; Jomaa, M.H.; Aberra Guebrou, S.; Homeyer, E.; Brucoli, G.; Bellessa, J. Lasing in a hybrid GaAs/silver Tamm structure. *Applied Physics Letters* **2012**, *100*, 121122. doi:10.1063/1.3697641.
29. Gazzano, O.; Michaelis de Vasconcellos, S.; Gauthron, K.; Symonds, C.; Voisin, P.; Bellessa, J.; Lemaître, A.; Senellart, P. Single photon source using confined Tamm plasmon modes. *Applied Physics Letters* **2012**, *100*, 232111. doi:10.1063/1.4726117.
30. Gessler, J.; Baumann, V.; Emmerling, M.; Amthor, M.; Winkler, K.; Höfling, S.; Schneider, C.; Kamp, M. Electro optical tuning of Tamm-plasmon exciton-polaritons. *Applied Physics Letters* **2014**, *105*, 181107. doi:10.1063/1.4901023.
31. Timofeev, I.V.; Arkhipkin, V.G.; Vetrov, S.Y.; Zyryanov, V.Y.; Lee, W. Enhanced light absorption with a cholesteric liquid crystal layer. *Optical Materials Express* **2013**, *3*, 496. doi:10.1364/OME.3.000496.
32. Vetrov, S.Y.; Pyatnov, M.V.; Timofeev, I. Surface modes in "photonic cholesteric liquid crystal–phase plate–metal" structure. *Optics Letters* **2014**, *39*, 2743. doi:10.1364/OL.39.002743.
33. Timofeev, I.; Vetrov, S.Y. Chiral optical Tamm states at the boundary of the medium with helical symmetry of the dielectric tensor. *JETP Letters* **2016**, *104*, 380–383, [1608.01876]. doi:10.1134/S0021364016180119.
34. Rudakova, N.V.; Timofeev, I.; Pankin, P.S.; Vetrov, S.Y. Polarization-preserving anisotropic mirror on the basis of metal–dielectric nanocomposite. *Bulletin of the Russian Academy of Sciences: Physics* **2017**, *81*, 5–9. doi:10.3103/S1062873817010257.
35. Alù, A.; Silveirinha, M.G.; Salandrino, A.; Engheta, N. Epsilon-near-zero metamaterials and electromagnetic sources: Tailoring the radiation phase pattern. *Physical Review B* **2007**, *75*, 155410, [arXiv:cond-mat/0609220]. doi:10.1103/PhysRevB.75.155410.
36. Inampudi, S.; Adams, D.C.; Ribaudo, T.; Slocum, D.; Vangala, S.; Goodhue, W.D.; Wasserman, D.; Podolskiy, V.A. ?? -Near-zero enhanced light transmission through a subwavelength slit. *Physical Review B - Condensed Matter and Materials Physics* **2014**, *89*, 1–10. doi:10.1103/PhysRevB.89.125119.
37. Ciattoni, A.; Rizza, C.; Marini, A.; Di Falco, A.; Faccio, D.; Scalora, M. Enhanced nonlinear effects in pulse propagation through epsilon-near-zero media. *Laser and Photonics Reviews* **2016**, *10*, 517–525. doi:10.1002/lpor.201500326.
38. Kaipurath, R.P.M.; Pietrzyk, M.; Caspani, L.; Roger, T.; Clerici, M.; Rizza, C.; Ciattoni, A.; Di Falco, A.; Faccio, D. Optically induced metal-to-dielectric transition in Epsilon-Near-Zero metamaterials. *Nature Publishing Group* **2016**, pp. 1–7, [1601.07088]. doi:10.1038/srep27700.
39. Park, J.; Kang, J.H.; Liu, X.; Brongersma, M.L. Electrically Tunable Epsilon-Near-Zero (ENZ) Metafilm Absorbers. *Scientific Reports* **2015**, *5*, 15754. doi:10.1038/srep15754.
40. Liu, R.; Roberts, C.M.; Zhong, Y.; Podolskiy, V.A.; Wasserman, D. Epsilon-Near-Zero Photonics Wires. *ACS Photonics* **2016**, *3*, 1045–1052, [1604.04576]. doi:10.1021/acsphotonics.6b00120.
41. Davoyan, A.; Mahmoud, A.; Engheta, N. Optical isolation with epsilon-near-zero metamaterials. *Optics Express* **2013**, *21*, 3279–3286, [1212.2292]. doi:10.1364/OE.21.003279.
42. Luk, T.S.; De Ceglia, D.; Liu, S.; Keeler, G.A.; Prasankumar, R.P.; Vincenti, M.A.; Scalora, M.; Sinclair, M.B.; Campione, S. Enhanced third harmonic generation from the epsilon-near-zero modes of ultrathin films. *Applied Physics Letters* **2015**, *106*. doi:10.1063/1.4917457.
43. Vetrov, S.Y.; Bikbaev, R.G.; Rudakova, N.V.; Chen, K.p.; Timofeev, I. Optical Tamm states at the interface between a photonic crystal and an epsilon-near-zero nanocomposite. *Journal of Optics* **2017**, *19*, 085103. doi:10.1088/2040-8986/aa75fb.
44. Oraevsky, A.N.; Protsenko, I.E. Optical properties of heterogeneous media. *Quantum Electronics* **2001**, *31*, 252–256. doi:10.1070/QE2001v031n03ABEH001927.
45. Sihvola, A. *Electromagnetic mixing formulas and applications [Book Review]*; Vol. 0, The Institution of Engineering and Technology, 1999; p. 296.
46. Vetrov, S.Y.; Avdeeva, A.Y.; Bikbaev, R.G.; Timofeev, I. Traveling of light through a 1D photonic crystal containing a defect layer with resonant dispersion. *Optics and Spectroscopy* **2012**, *113*, 517–521. doi:10.1134/S0030400X12110070.
47. Maxwell Garnett, J.C. Colours in metal glasses, in metallic films, and in metallic solutions. II. *Philos. R. Soc. London* **1906**, *205*, 237–288.
48. Markel, V.A. Introduction to the Maxwell Garnett approximation: tutorial. *Journal of the Optical Society of America A* **2016**, *33*, 1244. doi:10.1364/JOSAA.33.001244.

49. Yeh, P. Electromagnetic propagation in birefringent layered media. *Journal of the Optical Society of America* **1979**, *69*, 742. doi:10.1364/JOSA.69.000742.
50. Brückner, R.; Sudzius, M.; Hintschich, S.I.; Fröb, H.; Lyssenko, V.G.; Leo, K. Hybrid optical Tamm states in a planar dielectric microcavity. *Physical Review B* **2011**, *83*, 033405. doi:10.1103/PhysRevB.83.033405.
51. Born, M.; Wolf, E. *Principles of Optics: Electromagnetic Theory of Propagation, Interference and Diffraction of Light (7th Edition)*; Cambridge University Press, 1999.
52. Joannopoulos, J.D.; Johnson, S.G.; Winn, J.N.; Meade, R.D. *Photonic Crystals: Molding the Flow of Light, Second Edition*; 2008; p. 304.